Contributed paper

OPTO-ELECTRONICS REVIEW **11**(4), 321–326 (2003)

InNAs – a new optoelectronic material for mid-infrared applications

M. OSIŃSKI*

Centre for High Technology Materials, University of New Mexico
313 Goddard SE, Albuquerque, New Mexico 87106-4343, USA

The InN_xAs_{1-x} alloy is a very promising, although so far almost completely unexplored, novel material for mid-IR emitters and detectors. InNAs/GaAs multiple quantum wells were grown by MOCVD on GaAs substrates, using dimethylhydrazine (DMHy) as nitrogen precursor. The crystalline quality and solid phase composition were evaluated by high-resolution x-ray diffraction. The nitrogen content in InNAs wells was determined to be 18%. The measurements indicate high quality of quantum-well structures. The peak photoluminescence emission wavelengths of ~6.5 µm at 30 K and ~7.2 µm at 193 K are the longest reported so far for dilute nitride semiconductors.

Keywords: InNAs, dilute nitrides, MOCVD, dimethylhydrazine, multiple quantum wells, mid-infrared emitters.

1. Introduction

Semiconductor lasers and detectors operating in the mid-IR (2–8 µm) wavelength range are important for a variety of applications. Mid-IR sources are needed for remote detection of chemical vapours and liquids, environmental sensing, and trace gas monitoring. Many of these applications may require low cost solutions and operation over wide temperature range, ranging from cryogenic to room temperature, or at the very least, an operation temperature consistent with thermoelectric cooling (greater than ~240 K). Due to their compactness, ruggedness, reliability, and high efficiency, semiconductor lasers are by far preferred over any other types of lasers.

Most of the prior work on mid-IR diode laser emitters focused on using group-III-antimonide-based materials. Unfortunately, due to small band offset in this material system, operation of antimonide-based mid-IR diode lasers has been limited to cryogenic temperatures. While non-cryogenic operation up to 290 K is achievable with optical pumping [1], the maximum cw operation temperature of electrically pumped devices is only 195 K [2]. An alternative approach, relying on intersubband transitions in GaAs/AlGaAs quantum cascade lasers [3], requires very complicated multilayer structures with very stringent requirements of epitaxial growth precision, which results in high cost of these devices and makes it practically impossible to reach high output power levels. Moreover, even though the cw operation of quantum cascade lasers at room temperature has been reported very recently [4], the optical output power is still very small (3 mW at 312 K), and the output wavelength is very long (9.1 µm), longer than required for most mid-IR applications.

The InN_xAs_{1-x} alloy is a very promising, although so far almost completely unexplored, novel material for mid-infrared (2–8 µm) emitters and detectors. The room-temperature bandgap of InAs is 0.36 eV (3.44 µm). As with other dilute nitrides, incorporation of nitrogen into the host InAs crystal was predicted [5] to cause a significant shrinking (giant bowing) of the fundamental bandgap, although prior to our work this has been confirmed experimentally only for $x < 6\%$ [6,7]. Our recent results extend this range considerably to $x \approx 18\%$ [8–10].

InN_xAs_{1-x} can be lattice-matched to GaAs when $x = 38\%$ [11]. The large band offset between InNAs wells and GaAs barriers makes it particularly attractive for increasing the maximum temperature of cw operation and reducing temperature sensitivity of mid-IR lasers. If needed, even larger barriers can be obtained in the InNAs/AlGaAs system lattice-matched to GaAs.

2. MOCVD growth of InNAs on GaAs

With a single exception of recently reported MOCVD growth of InNAs using plasma cracked ammonia source [12], all studies of InNAs growth utilized plasma-source MBE [11,13], and related techniques, such as gas-source MBE with an rf-coupled plasma nitrogen source [7,14]. Recently, we have succeeded in growing InNAs on GaAs by MOCVD, using for the first time the dimethylhydrazine (DMHy) as nitrogen precursor [8].

Our material was grown in a Thomas Swan vertical MOCVD reactor at 60 Torr. Arsine and trimethylgallium were used during the growth of GaAs buffer, barrier, and cap layers. InNAs films were grown using trimethylindium, tertiarybutylarsine and DMHy as source materials. The metalorganic precursors were transported into the reactor chamber using hydrogen carrier gas. Before the growth,

*e-mail: osinski@chtm.unm.edu

epi-ready (100) n^+-GaAs substrates were deoxidised at 760°C for 5 minutes. 500 nm GaAs buffer layer was grown at 680°C. Subsequently, the growth temperature T_g was lowered to 500°C for the growth of InNAs/GaAs multiple quantum well (MQW) structures and the GaAs capping layer.

The growth rate was kept constant at 7.5 Å/s and 1.25 Å/s for GaAs and InNAs films, respectively. The mole fraction of DMHy to total group-V sources in the vapour phase was maintained between 0.95 and 0.975, corresponding to DMHy flow rate of 600–900 sccm.

3. X-ray characterisation of InNAs/GaAs multiple quantum wells

We have investigated crystalline quality, composition, and thicknesses of grown layers using high-resolution x-ray diffraction (HRXRD) Philips MRD triple axis apparatus. The system is equipped with a computer-controlled motorized goniometer, which enables the optimisation of all scattering angles with angular step sizes of 10^{-4} for the angles of incidence and reflection. A four-bounce Ge(220) Bartels-type monochromator was used to collimate the Cu $K_{\alpha 1}$ x-ray incident beam with an angular divergence $\Delta\omega$ = 12 arcsec. In order to maintain the $\Delta(2\theta)$ = 12 arcsec resolution at the detector, the diffracted beam was passed through a triple-bounce channel-cut analyser crystal.

Figure 1 shows HRXRD spectra of two multiple-quantum-well (MQW) structures grown under otherwise identical conditions, except for the presence of DMHy during the well layer growth. Sample DE218 (top scan) contained InAs/GaAs well layers, while sample DE315 (middle scan) contained InNAs/GaAs MQWs. Both samples were capped with 234-nm-thick layer of GaAs. Comparison of the two scans clearly reveals vast improvement in quality of the nitrogen-containing sample, which we attribute to a reduced lattice-constant mismatch between InNAs and GaAs, compared to InAs/GaAs system.

The FWHM of the $m = 0$ InNAs peak in Fig. 1 (middle scan) is 43 arcsec, which together with a clearly resolved spectrum displaying up to 14 diffraction orders indicates high crystalline quality of the sample. The FWHM of the $m = -3$ satellite peak of sample DE315 is 47 arcsec, comparing very favourably to 280 arcsec in $InN_{0.06}As_{0.94}$/InGaAsP MQWs grown on InP [7]. The satellite peaks wash out in the case of InAs/GaAs MQWs (top scan), revealing poorer interface flatness and partial relaxation.

The HRXRD spectra of sample DE315 were analysed using Bede Scientific Instruments RADS dynamic simulation software, assuming cubic InN and InAs lattice parameters, validity of Vegard's law, and fully coherent, pseudomorphic growth. As shown in Fig. 1, the nitrogen composition of 18.5% resulted in a very good fit. Using the same simulation, the well and barrier layer thicknesses were determined as 1.1 nm and 35 nm, respectively.

In order to determine whether the assumption of fully strained InNAs/GaAs quantum wells was correct, we performed state-of-the-art two-dimensional x-ray reciprocal space mapping (2D-RSM) on the same sample DE315. 2D-RSM is a powerful defect-sensitive technique that can

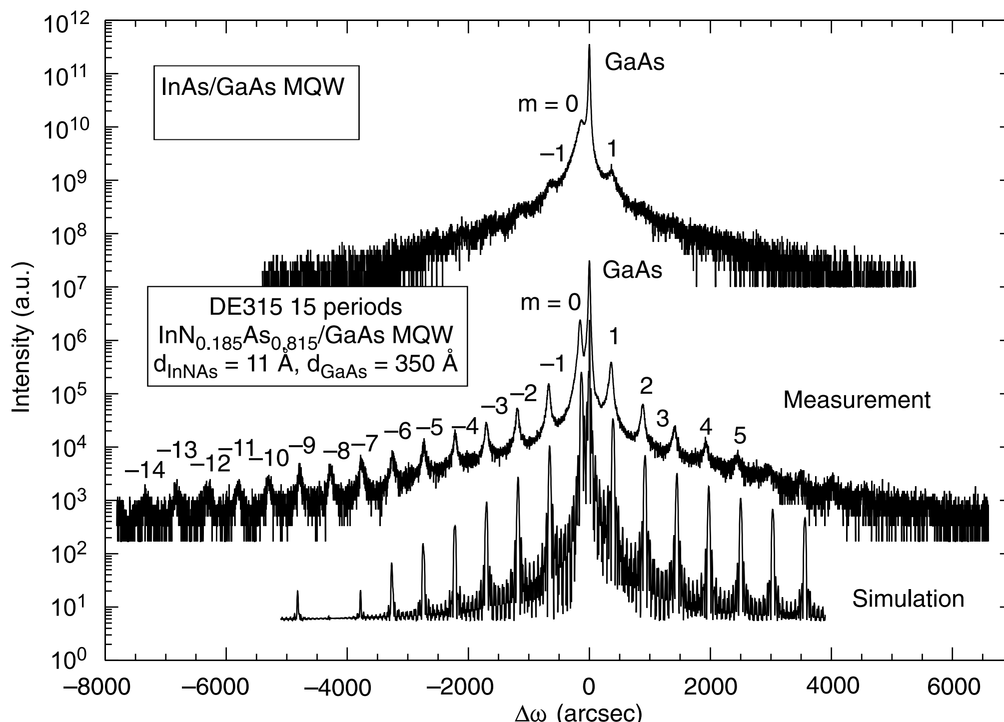

Fig. 1. ω-2θ scans of (004) reflections for 15-period MQW samples with InAs wells (top scan) and InNAs wells (middle scan). The bottom scan represents the simulated HRXRD spectrum.

 © 2003 COSiW SEP, Warsaw

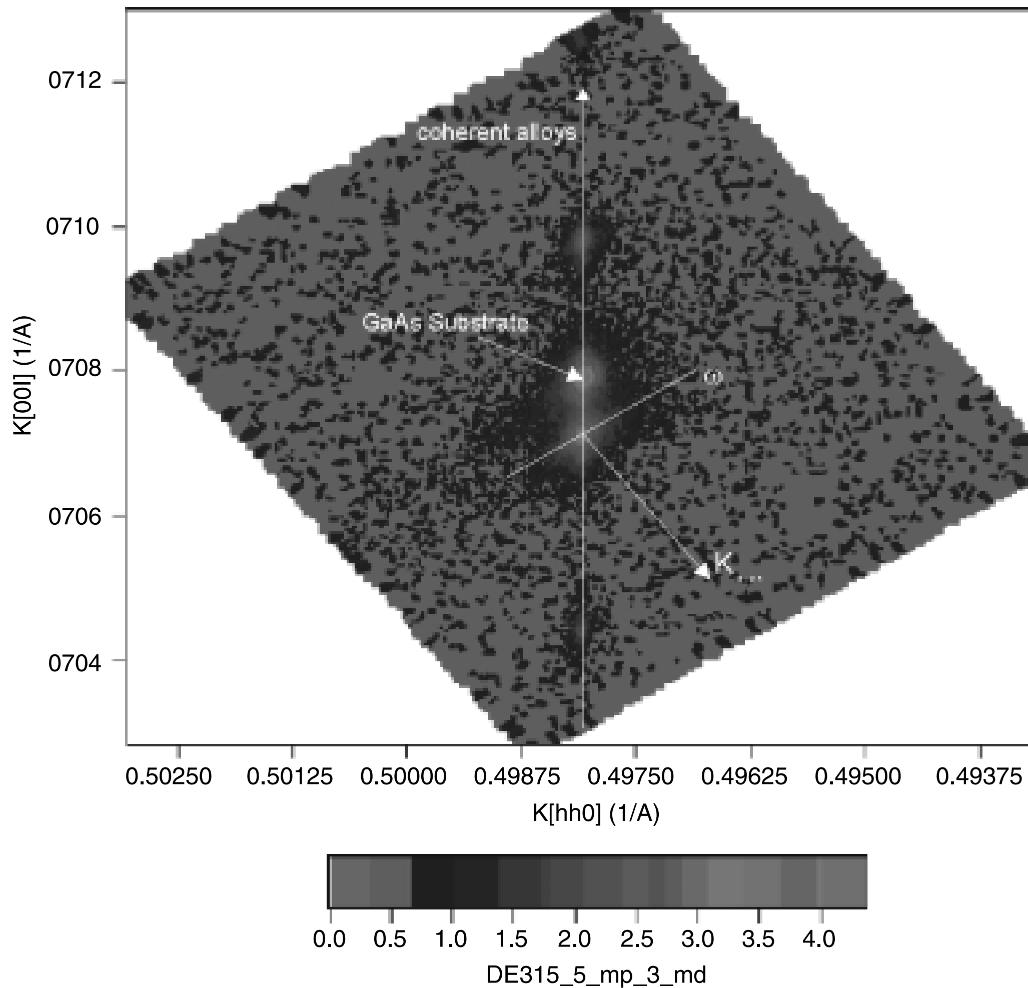

Fig. 2. Reciprocal space mapping around the $\overline{22}4$ reciprocal lattice point for sample DE315. Two diffuse elliptical disks of very small intensity on either side of the [00l] rod along the direction are due to a defective region in the sample, not to strain relaxation.

determine the degree of relaxation in strained heterostructures [15,16]. It involves a series of double-crystal rocking curve scans in $\omega/2\theta$ with an offset in ω value. The projection of the intensity along the $k[001]$ direction provides information regarding growth-direction lattice constant, chemical inhomogeneity, and epilayer thicknesses. The width of in-plane projection along $k[hh0]$ provides structural information about in-plane lattice constant and crystallographic misorientations.

Figure 2 shows the results obtained for 2D-RSM around the asymmetric $\overline{22}4$ reciprocal lattice point (RSM $\overline{22}4$ reflection). High quality of the specimen is evidenced by the very small size of the broadened intensity features.

4. HRTEM characterisation of InNAs/GaAs multiple quantum wells

High quality of InNAs/GaAs MQWs is also confirmed by cross-sectional TEM measurements, illustrated in Fig. 3. The thicknesses of InNAs wells and GaAs barriers derived from the x-ray diffraction analysis are consistent with those shown in Fig. 3.

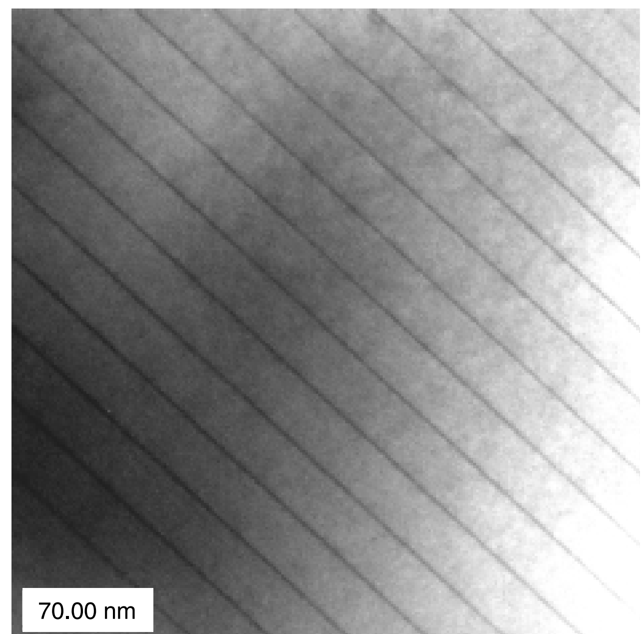

Fig. 3. Cross-sectional bright-field TEM image of 15-period InNAs/GaAs MQW sample DE315.

A direct confirmation of the presence of nitrogen in quantum wells can be obtained using the electron energy-loss spectroscopy (EELS) in our high-resolution transmission electron microscope (HRTEM). EELS involves an analysis of the energy distribution of electrons that have interacted inelastically with the specimen. These inelastic collisions can reveal important information about the electronic structure of the specimen atoms, including their identification, their bonding and nearest-neighbour distributions, and their dielectric response. EELS can be applied with several techniques, but always involves the bombardment of a sample with a monoenergetic beam of electrons. The electrons impinging on the sample may lose energy by a variety of mechanisms. These losses can reveal the composition of the sample in TEM or STEM. Plasmon losses are a frequent cause of energy loss. Plasmons are collective excitations of the electron gas in the material and are typically several eV in energy. Phonon losses can also occur, but they are much smaller, and the energy spread of the monoenergetic beam must be particularly small to detect such losses.

In order to determine the electron energy spectrum, we use a magnetic prism spectrometer which, when interfaced to a TEM, creates another form of analytical electron microscope (AEM). The magnetic prism is a simple, but highly sensitive, device with resolving power of approximately 1 eV, even when the energy of incident electron beam is as large as 400 keV. Using this setup, we performed composition mapping of sample DE315. Figure 4 shows perfect coincidence of bright lines tracing the regions rich in nitrogen and indium inside the quantum wells.

5. Photoluminescence measurements

The photoluminescence (PL) setup used to characterise the InNAs/GaAs quantum wells included a Coherent Innova 300 Ar-ion laser source, with combined 514 nm and 488 nm lines pumping a Schwartz Electro-Optics Titan-ML

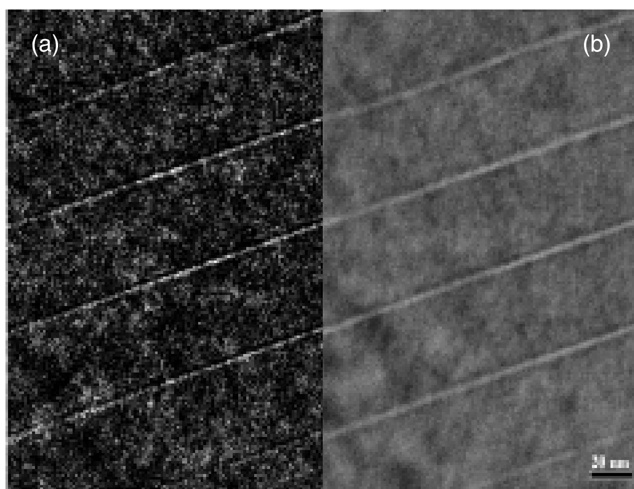

Fig. 4. Electron energy loss spectroscopy (EELS) analysis of sample DE315. (a) Nitrogen mapping; (b) Indium mapping.

tunable Ti:sapphire laser, a Nicolet Magna-IR 760 Fourier Transform infrared spectrometer, and a Nicolet MCT-B cooled detector. The output power from the argon-ion laser was 7.5 W, while the output power incident on the sample from the Ti:sapphire laser tuned to 890 nm was 320 mW, illuminating a spot with ~1 mm diameter. Rather than relying on temperature-controller readings, we used a bulk InSb sample for *in-situ* temperature calibration of illuminated sample.

Our initial experiments with as-grown InNAs/GaAs triple QW samples resulted in no detected PL signal. The samples were then annealed at 550°C for 5 min using a rapid thermal annealer, which activated the PL. Some samples, however, did emit a PL signal even without annealing. During the measurements, both InNAs and bulk InSb samples were located in close proximity inside the cryostat. Within the temperature range where InSb emitted a PL signal (up to 110 K), we assumed the actual temperature of InNAs sample to be the same as the temperature of InSb. The data taken at 39, 510, and 110 K were then used to estimate the Varshni parameters for $InN_{0.18}As_{0.82}$, yielding the following results: $E_g(0)$ = 0.1953 eV, $\alpha = 2.2\times10^{-4}$ eV/K, and β = 64 K. We then extrapolated the Varshni relationship beyond 100 K. By fitting the PL emission peak wavelengths to the wavelength vs. temperature curve, we determined the actual sample temperatures to be 115 K, 143 K, 161 K, and 193 K.

Figure 5 shows the measured PL spectra for as-grown triple QW InNAs/GaAs sample DE233 not subjected to any annealing. At 39 K, the peak emission wavelength was ~6.5 µm (190 meV), and the FWHM of the PL spectrum was ~3.5 µm (110 meV). Clear PL signals centered at ~7 µm, with FWHM narrowing down to ~2 µm (~65 meV), were observed up to 193 K. The peak emission wavelength of ~7 µm is the longest reported so far for dilute nitride semiconductors.

The distinct features shown in the spectra in Fig. 5 are due to absorption of the infrared light emitted by the sample as it passes through ambient air from the cryostat to the detector inside the FTIR spectrometer. The dip at 4.26 µm is due to CO_2 absorption, while the broad minima near 5.9 and 6.5 µm are caused by water vapour absorption in the ambient atmosphere. The maximum at 6.3 µm coincides with the water vapour transmission window.

6. Discussion

Recently, InNAs band structure calculations were reported, considering various possible arrangements of group-V atoms around an In atom [17]. For 17.6% nitrogen content, bandgaps ranging from 8 meV for maximally nitrogen-rich clusters to 251 meV for maximally As-rich clusters were predicted. Although the results in Ref. 17 are valid only for bulk unstrained InNAs, this wide bandgap range is consistent with our observation of broad PL emission spectra (Fig. 5). It is also very promising for widely tunable mid-IR lasers.

 © 2003 COSiW SEP, Warsaw

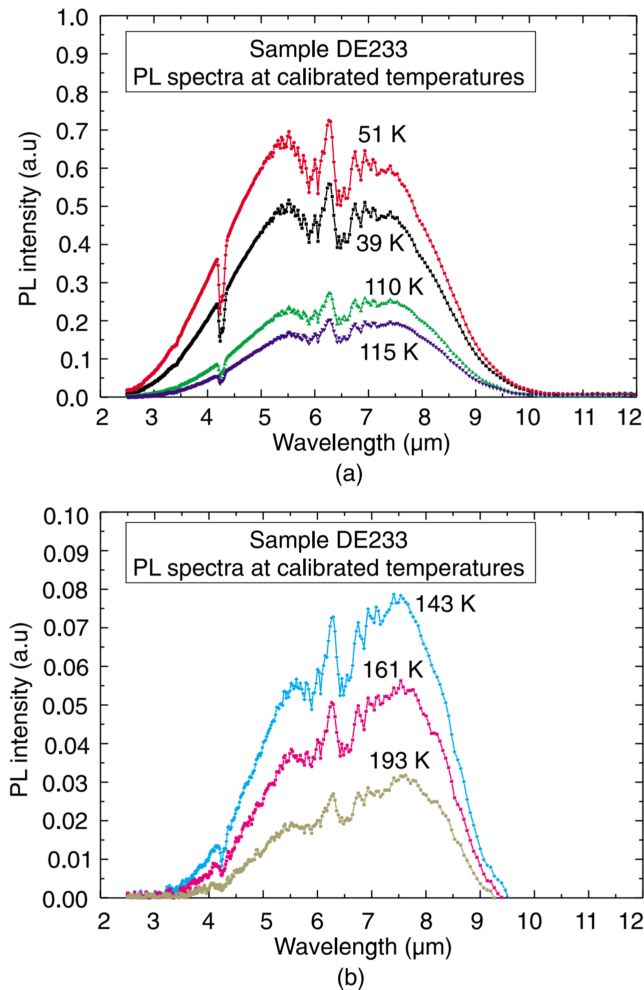

Fig. 5. PL spectra of sample DE233 containing a triple-quantum-well 2.2-nm-InNAs/35-nm-GaAs structure. The temperatures indicated are actual sample temperatures determined by using the Varshni formula for the PL emission peak from a bulk InSb sample placed in the cryostat, determining Varshni parameters for InNAs, and extrapolating beyond InSb emission temperatures.

7. Conclusions

We have successfully grown InNAs/GaAs multiple-quantum-well structures by MOCVD using dimethylhydrazine (DMHy). The crystalline quality and solid phase composition were evaluated by high-resolution x-ray diffraction. The nitrogen content in InNAs wells was determined to be 18%. High-resolution transmission electron microscopy (HRTEM) was used to study crystalline quality and to map the spatial distribution of indium and nitrogen using electron energy-loss spectroscopy (EELS). All these measurements indicate high quality of quantum-well structures. PL measurements confirm that the bandgap energy of InNAs is significantly lower than that of InAs. The peak emission wavelengths of ~6.5 µm at 30 K and ~7.2 µm at 193 K are the longest reported so far for dilute nitride semiconductors.

Acknowledgments

The results described in this paper have been obtained in collaboration with Dr. Abdel-Rahman A. El-Emawy (MOCVD crystal growth) and Dr. Huifang Xu (TEM measurements), as well as graduate students Noppadon Nuntawong and Hongjun Cao, all at the University of New Mexico. Support from the U.S. Air Force Office of Scientific Research under the Optoelectronics Research Centre program is gratefully acknowledged.

References

1. C.L. Felix, W.W. Bewley, I. Vurgaftman, R.E. Bartolo, D.W. Stokes, J.R. Meyer, M.J. Yang, H. Lee, R.J. Menna, R.U. Martinelli, D.Z. Garbuzov, J.C. Connolly, M. Maiorov, A.R. Sugg, and G.H. Olsen, "Mid-infrared W quantum-well lasers for noncryogenic continuous-wave operation", *Appl. Opt.* **40**, 806–811 (2001).
2. W.W. Bewley, H. Lee, I. Vurgaftman, R.J. Menna, C.L. Felix, R.U. Martinelli, D.W. Stokes, D.Z. Garbuzov, J.R. Meyer, M. Maiorov, J.C. Connolly, A.R. Sugg, and G.H. Olsen, "Continuous-wave operation of λ = 3.25 µm broadened-waveguide W quantum-well diode lasers up to T = 195 K", *Appl. Phys. Lett.* **76**, 256–258 (2000).
3. C. Gmachl, F. Capasso, D.L. Sivco, and A.Y. Cho, "Recent progress in quantum cascade lasers and applications", *Rep. Progress Phys.* **64**, 1533–1601 (2001).
4. M. Beck, D. Hofstetter, T. Aellen, J. Faist, U. Oesterle, M. Ilegems, E. Gini, and H. Melchior, "Continuous wave operation of a mid-infrared semiconductor laser at room temperature", *Science* **295**, 301–305 (2002).
5. T. Yang, S. Nakajima, and S. Sakai, "Tight-binding calculation of electronic structures of InNAs ordered alloys", *Jpn. J. Appl. Phys.* **36**, L320 (1997).
6. H. Naoi, Y. Naoi, and S. Sakai, "MOCVD growth of InAsN for infrared applications", *Solid-State Electron.* **41**, 319–321 (1997).
7. J.S. Wang, H.H. Lin, L.W. Song, and G.R. Chen, "Growth of InAsN/InGaAs(P) quantum wells on InP by gas source molecular beam epitaxy", *J. Vac. Sci. & Technol.* **B19**, 202 (2001).
8. A.A. El-Emawy, H.J. Cao, E. Zhmayev, J.H. Lee, D. Zubia, and M. Osiński, "MOCVD growth of InN_xAs_{1-x} on GaAs using dimethylhydrazine", *Phys. Stat. Sol. (b)* **228**, 263–267 (2001).
9. H.J. Cao, N. Nuntawong, A.A. El-Emawy, and M. Osiński, "Characterisation of MOCVD-grown InNAs/GaAs quantum wells", *23rd Annual Conf. on Lasers and Electro-Optics CLEO 2002*, Long Beach, CA, 19-24 May 2002, 653–654 (2002).
10. M. Osiński, N. Nuntawong, H.J. Cao, E. Zhmayev, and A.A. El-Emawy, "MOCVD growth and characterisation of InNAs on GaAs - a new narrow-gap semiconductor (Invited Paper)", *Proc. Narrow Bandgap Optoelectronic Materials and Devices Symp., Electrochem. Soc. Meeting*, Salt Lake City, UT, 21 Oct. 2002, 60–71 (2002).
11. Y.C. Kao, T.P.E. Broekaert, H.Y. Liu, S. Tang, I.H. Ho, and G.B. Stringfellow, "Lattice-matched InAsN (x = 0.38) on GaAs grown by molecular beam epitaxy", *Proc. MRS Symp.*

III-Nitride, SiC and Diamond Materials for Electronic Devices, San Francisco, CA, 8-12 April, 335–340 (1996).
12. H. Naoi, D. M. Shaw, Y. Naoi, G.J. Collins, and S. Sakai, "Growth of InNAs by low-pressure metalorganic chemical vapour deposition employing microwave-cracked nitrogen and *in situ* generated arsine radicals", *J. Cryst. Growth* **222**, 511–517 (2001).
13. R. Beresford, K.S. Stevens, and A.F. Schwartzman, "Microstructure and composition of InAsN alloys grown by plasma-source molecular beam epitaxy", *J. Vac. Sci. & Technol.* **B16**, 1293 (1998).
14. W.K. Hung, K.S. Cho, M.Y. Chern, Y.F. Chen, D.K. Shih, H.H. Lin, C.C. Lu, and T.R. Yang, "Nitrogen-induced enhancement of the electron effective mass in InN_xAs_{1-x}", *Appl. Phys. Lett.* **80**, 796–798 (2002).
15. P.F. Fewster, V. Holy, and N.L. Andrew, "Detailed structural analysis of semiconductors with X-ray scattering", *Materials Science in Semiconductor Processing* **4**, 475–481 (2001).
16. S. Pereira, M.R. Correia, E. Pereira, K.P. O'Donnell, E. Alves, A.D. Sequeira, N. Franco, I.M. Watson, and C.J. Deatcher, "Strain and composition distributions in wurtzite InGaN/GaN layers extracted from x-ray reciprocal space mapping", *Appl. Phys. Lett.* **80**, 3913–3915 (2002).
17. N. Tit and M.W.C. Dharma-wardana, "Electronic structure of InN_xAs_{1-x} alloys from tight-binding calculations", *Appl. Phys. Lett.* **76**, 3576–3578 (2000).

 © 2003 COSiW SEP, Warsaw